AIAA JOURNAL
Vol. 42, No. 7, July 2004

Implicit Gas-Kinetic Bhatnagar–Gross–Krook Scheme for Compressible Flows

Ong Jiunn Chit*
University Putra Malaysia, 43400, Serdang, Selangor D.E., Malaysia
Ashraf Ali Omar† and Waqar Asrar‡
International Islamic University Malaysia, Jalan Gombak, 53100, Kuala Lumpur, Malaysia
and
Megat Mohammad Hamdan§
University Putra Malaysia, 43400, Serdang, Selangor D.E., Malaysia

A gas-kinetic scheme based on the Bhatnagar–Gross–Krook (BGK) model is developed for two-dimensional compressible inviscid flowfields. The BGK scheme is an approximate Riemann solver that uses the collisional Boltzmann equation as the governing equation for flow evolutions. For efficient computations, particle distribution functions in the general solution of the BGK model are simplified and used for the flow simulations. High-order accuracy is achieved via the reconstruction of flow variables using the MUSCL interpolation technique. For steady-state problems, the approximate factorization–alternating direction implicit implicit time integration method is adopted, which is preferable to a multistage Runge–Kutta method. To investigate the computational characteristics of BGK scheme in detail, it has been applied to various two-dimensional numerical experiments. The results, compared with some typical schemes, such as the Steger–Warming flux vector splitting and Roe flux difference splitting, as well as exact solutions, are found to be robust and accurate, and to have high resolution at discontinuities such as shock waves.

I. Introduction

MANY numerical schemes have been developed in the past for compressible inviscid flow simulations. The main goal is to design a numerical scheme that fulfills all of the ideal computational requirements, which are a high degree of accuracy, robustness, and efficiency. Although great effort has been put forth and advances have been achieved toward this goal, however, no scheme seems to be perfect enough to meet all of the mentioned conditions. Among the schemes that are notable and successful are the Godunov-type schemes and flux-vector-splitting schemes. In the family of Godunov-type schemes, Roe's flux-difference-splitting (FDS) scheme[1] is the most popular because of its accuracy for compressible inviscid and viscous flow simulations. However, the occurrence of transverse shock instability and negative internal energy of Godunov-type schemes hinder their usage in the computation of high-speed flows with strong shock waves and expansion fans.[2] For this reason, contemporary development of numerical schemes is focused on combining the accuracy of Godunov-type schemes and the robustness of flux-vector-splitting (FVS) schemes.

In conventional numerical schemes, the Euler equations are discretized for the solutions of compressible inviscid flows. In addition to these schemes, several gas-kinetic schemes have been developed based on the Boltzmann equation (see Ref. 3). A particular strength of kinetic schemes lies precisely where Godunov-type FDS schemes often fail, such as for carbuncle phenomena, entropy condition, and positivity (Refs. 4 and 5; data also available online by Xu, K., "Gas Evolution Dynamics in Godunov-Type Schemes," at URL: http//math.ntnu.no/conservation/1998/025.html). There are mainly two kinds of gas-kinetic schemes, and the differences lie within the governing equations used in the gas evolution stage. One of the well-known kinetic schemes is the kinetic FVS (KFVS), which is based on the collisionless Boltzmann equation, and the other is based on the collisional Bhatnagar–Gross-Krook (BGK) model (see Ref. 6). Like any other FVS method, the KFVS scheme is very diffusive and less accurate in comparison with the Roe-type Riemann solver. The diffusivity of the FVS schemes is mainly due to the particle or wave-free transport mechanism, which sets the Courant–Friedrichs–Lewy (CFL) time step equal to particle collision time.[7] To reduce diffusivity, particle collisions have to be modeled and implemented into the gas evolution stage. One of the distinct approaches to take particle collision into consideration in gas evolution can be found by Xu.[3] In this method, the collision effect is considered by the BGK model as an approximation of the collision integral in the Boltzmann equation. It is found that this gas-kinetic BGK scheme possesses accuracy that is superior to the FVS schemes and avoids the anomalies of Godunov-type schemes (Refs. 2, 3, 8, and 9 and cited Ku website).

In the past decade, the gas-kinetic BGK scheme has attracted much attention and matured, successfully simulating compressible inviscid flows and other applications. Recent advancements include the introduction of Jameson's symmetric limited positive formulation to construct high-order BGK scheme by Xu[3] in 1995. From 1996 until 1999, Xu[7,10] and Lian and Xu[11] successfully applied the BGK scheme to solve shallow water equations, ideal magnetohydrodynamics equations, chemical reactions, and two-phase fluid (data also available online by Xu, K., "Unsplitting BGK-type Schemes for Shallow Water Equations," at URL: http//math.ntnu.no/conservation/1996/035.html). In 2000, Chae et al.[2] proposed an improved gas-kinetic BGK scheme by including the Prandtl number correction into flux calculations. In 2002, Ruan and Jameson[12] extended the gas-kinetic BGK scheme to three-dimensional compressible flows for the first time. Most recently, Kunik et al.[13] solved the ultrarelativistic Euler equations using the BGK scheme.

Received 29 April 2003; revision received 4 January 2004; accepted for publication 15 January 2004.

*Graduate Research Assistant, Department of Aerospace Engineering, Faculty of Engineering.
†Assistant Professor, Department of Mechanical Engineering, Faculty of Engineering.
‡Associate Professor, Department of Mechanical Engineering, Faculty of Engineering; waqar@iiu.edu.my.
§Associate Professor, Department of Mechanical and Manufacturing Engineering, Faculty of Engineering.

This paper is organized as follows. The governing equations for the two-dimensional compressible inviscid flows in Cartesian and generalized coordinates are presented. The construction of the gas-kinetic BGK scheme is also addressed. Then, a proposed method of reconstructing the initial solutions is described. An implicit time integration method is adopted for solving the gas-kinetic BGK scheme. Next, the developed schemes are applied to various numerical tests to investigate their essential features. The computational results are compared with the exact solutions and numerical results from other schemes, such as Steger-Warming FVS scheme and Roe's FDS scheme. Last, concluding remarks are made.

II. Numerical Methods

A. Governing Equations

The two-dimensional Euler equations in Cartesian coordinates are written as

$$\frac{\partial W}{\partial t}+\frac{\partial F}{\partial x}+\frac{\partial G}{\partial y}=0 \tag{1}$$

where

$$W=\begin{bmatrix}\rho\\ \rho U\\ \rho V\\ \rho\varepsilon\end{bmatrix},\qquad F=\begin{bmatrix}\rho U\\ \rho U^2+p\\ \rho UV\\ (\rho\varepsilon+p)U\end{bmatrix},\qquad G=\begin{bmatrix}\rho V\\ \rho UV\\ \rho V^2+p\\ (\rho\varepsilon+p)V\end{bmatrix} \tag{2}$$

In Eq. (1), ρ, ρU, ρV, and $\rho\varepsilon$ are the macroscopic mass, x momentum, y momentum, and total energy density, respectively, and p is the pressure.

Equation (1) can be transformed from Cartesian coordinates (x, y) into curvilinear coordinates (ξ, η) as

$$\frac{\partial \hat{W}}{\partial t}+\frac{\partial \hat{F}}{\partial \xi}+\frac{\partial \hat{G}}{\partial \eta}=0 \tag{3}$$

where

$$\hat{W}=J^{-1}W,\qquad \hat{E}=J^{-1}(\xi_x F+\xi_y G)$$

$$\hat{G}=J^{-1}(\eta_x F+\eta_y G) \tag{4}$$

In Eq. (4), $J=(\xi_x\eta_y-\xi_y\eta_x)$ is the Jacobian of transformation. The manner in which the metrics ξ_x, ξ_y, η_x, and η_y and the Jacobian of transformation J are evaluated is detailed by Hoffmann and Chiang.[14]

B. Gas-Kinetic BGK Scheme

A standard gas-kinetic BGK scheme is based on the collisional Boltzmann equation (see Ref. 3), and it is written in two dimensions as

$$\frac{\partial f}{\partial t}+u\frac{\partial f}{\partial x}+v\frac{\partial f}{\partial y}=Q(f, f) \tag{5}$$

where f is a real particle distribution function, u and v are the particle velocities, and the right-hand side stands for the collision term. The collision term is an integral function that accounts for the binary collisions. The BGK model of the Boltzmann equation is realized when a relaxation model (see Ref. 3) is suggested as an approximation for the complicated collision term in Eq. (5), which can be written as

$$\frac{\partial f}{\partial t}+u\frac{\partial f}{\partial x}+v\frac{\partial f}{\partial y}=\frac{(g-f)}{\tau} \tag{6}$$

where g is an equilibrium particle distribution function that f approaches through particle collisions within a collision timescale τ. Both f and g are functions of space x and y, time t, particle velocities u and v, and ς. Here ς is a K-dimensional vector that accounts for the internal degrees of freedom such as molecular rotation and vibrations. The dimensional vector K is related to the specific heat ratios and the space dimension by the relation $K=(4-2\gamma)/(\gamma-1)$, where for a diatomic gas, $\gamma=1.4$.

The relations between the densities of mass ρ, momentum ρU and ρV, and total energy ε with the distribution function f are derived from the following moment relation:

$$\begin{pmatrix}\rho\\ \rho U\\ \rho V\\ \varepsilon\end{pmatrix}=\int f\boldsymbol{\Psi}\,\mathrm{d}\Xi \tag{7}$$

where $\mathrm{d}\Xi=\mathrm{d}u\,\mathrm{d}v\,\mathrm{d}\varsigma$ is the volume element in the phase space and $\boldsymbol{\Psi}$ is the vector of moments

$$\boldsymbol{\Psi}=\begin{pmatrix}1\\ u\\ v\\ \frac{1}{2}(u^2+v^2+\varsigma^2)\end{pmatrix} \tag{8}$$

With the moment relation defined in Eq. (7), a similar approach could be adopted in obtaining the numerical fluxes across cell interfaces, and they are given as

$$F_x=\int uf\boldsymbol{\Psi}\,\mathrm{d}\Xi,\qquad G_y=\int vf\boldsymbol{\Psi}\,\mathrm{d}\Xi \tag{9}$$

where F_x and G_y are the physical flux in the x and y directions, respectively. In addition, within the physical constraint of the conservation of mass, momentum, and energy during particle collisions, the following compatibility condition has to be satisfied:

$$\int\frac{(g-f)}{\tau}\boldsymbol{\Psi}\,\mathrm{d}\Xi=0 \tag{10}$$

at any point in space and time. This assumption will lead to the two-dimensional Euler equations.

A general solution f of Eq. (6) at the cell interface $(x_{i+1/2}, y_j)$ in two dimensions is obtained as

$$f(x, y, t, u, v, \varsigma)=\frac{1}{\tau}\int_0^t g(x', y', t, u, v, \varsigma)\exp\left[\frac{-(t-t')}{\tau}\right]\mathrm{d}t'$$

$$+\exp\left(\frac{-t}{\tau}\right)f_0(x-ut, y-vt) \tag{11}$$

where $x'=x_{i+1/2}-u(t-t')$ and $y'=y_j-v(t-t')$ are particle trajectories and f_0 is the initial nonequilibrium distribution function at $t=0$. To construct the numerical flux from the solution of f in Eq. (11), two unknowns g and f_0 must be determined. Hence, by the discretization of the two distribution functions g and f_0 as proposed by Xu,[3] the following forms are obtained:

$$f_0=\begin{cases}g^l, & x<0\\ g^r, & x>0\end{cases} \tag{12}$$

$$g=g_0 \tag{13}$$

where g^l, g^r, and g_0 are local Maxwellian distribution function at the left, right, and middle of a cell interface, respectively. When the relation between the microscopic and macroscopic descriptions as described in Eq. (7) is used, the state variables that constitute the Maxwellian distribution function g^l, and g^r of Eq. (12) can be obtained as

$$\begin{pmatrix}\rho^*\\ \rho^*U^*\\ \rho^*V^*\\ \varepsilon^*\end{pmatrix}=\int g^*\boldsymbol{\Psi}\,\mathrm{d}\Xi \tag{14}$$

where the superscript asterisk denotes the left or right state variables at the cell interface. The Maxwellian g^* has the following form:

$$g^* = \rho^*(\lambda^*/\pi)^{(K+2)/2} \exp\{-\lambda^*[(u-U^*)^2 + (v-V^*)^2 + \varsigma^2]\} \tag{15}$$

Then, the parameters of the Maxwellian g_0 can be constructed by taking the limit of Eq. (11) as $t \to 0$ and substituting it into Eq. (10) at the cell interface $(x_{i+1/2}, y_j) = (0, 0)$ to obtain

$$\int g_0 \Psi \, d\Xi = \int f_0(-ut)\Psi \, d\Xi \begin{pmatrix} \rho_0 \\ \rho_0 U_0 \\ \rho_0 V_0 \\ \varepsilon_0 \end{pmatrix}$$

$$= \int_{u>0} g^l \Psi \, d\Xi + \int_{u<0} g^r \Psi \, d\Xi \tag{16}$$

The underlying physical assumption in the preceding equation is that the left and right moving particles collapse at a cell interface to form an equilibrium state g_0. Hence, the quantities with subscript 0 are termed equilibrium state variables at the cell interface, and they could be determined by taking the moments of the Maxwellian distribution function in Eq. (16). All of the moment calculations involved in the integration of the Maxwellian in phase space from negative infinity to zero or zero to positive infinity are expressed in term of exponential and error functions are found in Refs. 2, 3, and 8.

With all of the parameters for the Maxwellian distribution functions determined, the solution f of the BGK model at $(x_{i+1/2}, y_j) = (0, 0)$ in Eq. (11), Eqs. (12) and (13) are substituted together with the assumption of constant equilibrium state g_0 in space and time. The following form is obtained:

$$f(0, 0, t, u, v, \varsigma) = [1 - \exp(-t/\tau)]g_0 + \exp(-t/\tau) f_0(-ut, -vt) \tag{17}$$

With the definition of $\exp(-t/\tau) = \varphi$, the distribution function f is written as

$$f(0, 0, t, u, v, \varsigma) = (1-\varphi)g_0 + \varphi f_0(-ut, -vt) \tag{18}$$

For the first-order BGK scheme, the term φ is assumed as a constant, where $\varphi \in [0, 1]$. When the BGK scheme is extended to high order, the value of φ should depend on the real flow situations. This option is necessary to prevent numerical oscillations and to be physically correct in that it accounts for the nonequilibrium behavior of the gas flow in the discontinuity region. A possible choice for φ in a high-order scheme is to design a pressure-based stencil, such as the switch function in the Jameson–Schmidt–Turkel (JST) scheme (see Refs. 3, 7, and 12). The following form is chosen for the φ parameter when the scheme is extended to high order:

$$\varphi = 1 - \exp\left(-\beta \frac{|p_l - p_r|}{p_l + p_r}\right) \tag{19}$$

where β can be some constant.

Finally, the gas-kinetic BGK numerical flux across the cell interface in the x direction can be computed as

$$F_x = \int u \, f(0, 0, t, u, v, \varsigma)\Psi \, d\Xi$$

$$F_x = (1-\varphi)F_x^e + \varphi F_x^f \tag{20}$$

where F_x^e is the equilibrium flux function and F_x^f is the nonequilibrium or freestream flux function.

The numerical flux for the BGK scheme at the cell interface in the x direction is obtained from Eq. (20) as

$$F_{i+\frac{1}{2},j} = (1-\varphi)F^e_{i+\frac{1}{2},j} + \varphi F^f_{i+\frac{1}{2},j} \tag{21}$$

whereas the numerical flux at the cell interface in the y direction is obtained in a similar manner and the resulting relation is

$$G_{i,j+\frac{1}{2}} = (1-\varphi)G^e_{i,j+\frac{1}{2}} + \varphi G^f_{i,j+\frac{1}{2}} \tag{22}$$

C. Reconstruction Stage

For high-order spatial accuracy, a method known as the MUSCL approach[15] is adopted. To avoid spurious oscillations in the solution, a limiter is used to extrapolate the primitive variables at the cell interfaces. In this paper, van Leer's limiter is employed. Hence, the left and right states of the primitive variables ρ, U, V, and p at a cell interface could be obtained through the non linear reconstruction of the respective variables given as

$$Q_l = Q_{i,j} + \frac{1}{2}\phi\left(\frac{\Delta Q_{i+\frac{1}{2},j}}{\Delta Q_{i-\frac{1}{2},j}}\right)\Delta Q_{i-\frac{1}{2},j}$$

$$Q_r = Q_{i+1,j} - \frac{1}{2}\phi\left(\frac{\Delta Q_{i+\frac{3}{2},j}}{\Delta Q_{i+\frac{1}{2},j}}\right)\Delta Q_{i+\frac{1}{2},j} \tag{23}$$

where Q is a primitive variable and the subscript l and r correspond to the left and right side of a considered cell interface. In addition, $\Delta Q_{i+1/2,j} = Q_{i+1,j} - Q_{i,j}$. The van Leer limiter used in the reconstruction of flow variables in Eq. (23) is given as

$$\phi(\Omega) = (\Omega + |\Omega|)/(1+\Omega) \tag{24}$$

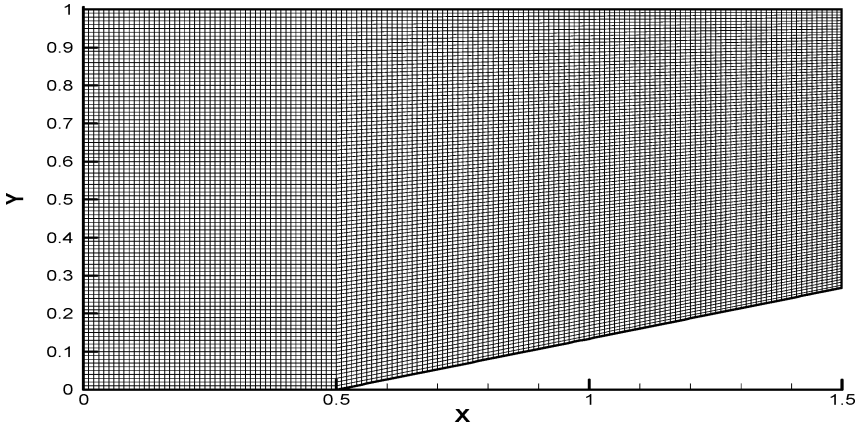

Fig. 1 Wedge problem grid with 151 × 101 grid points.

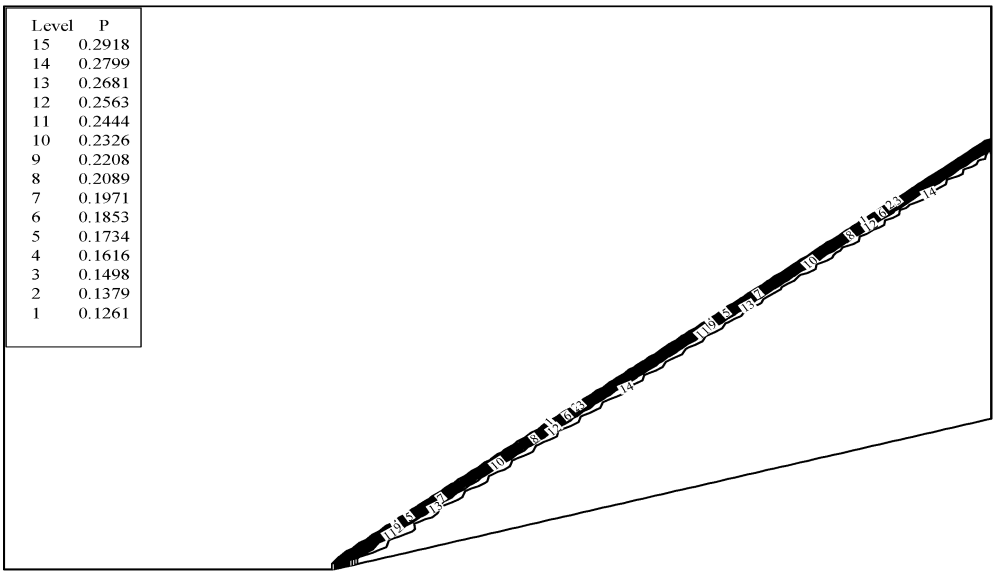

a) BGK scheme

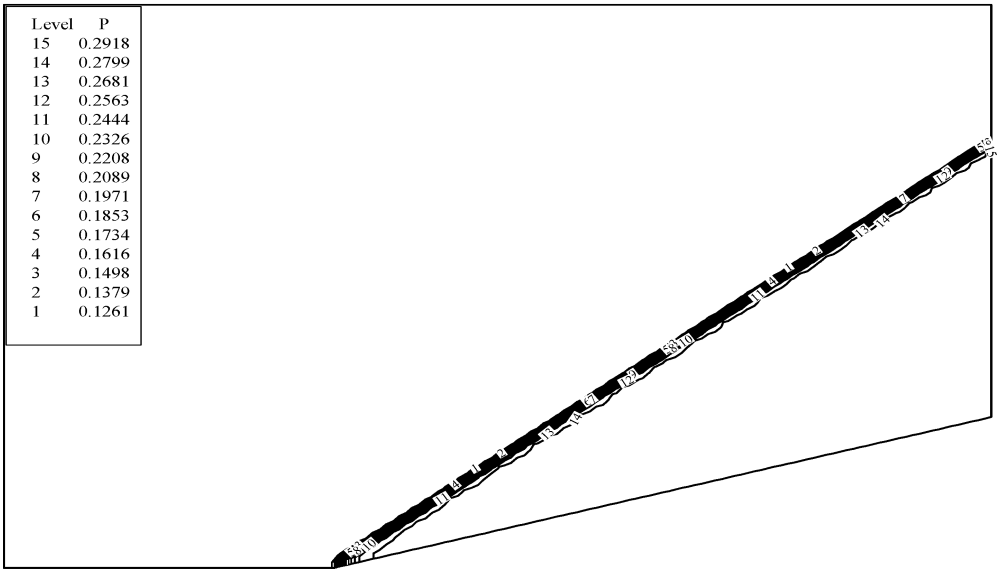

b) Roe scheme

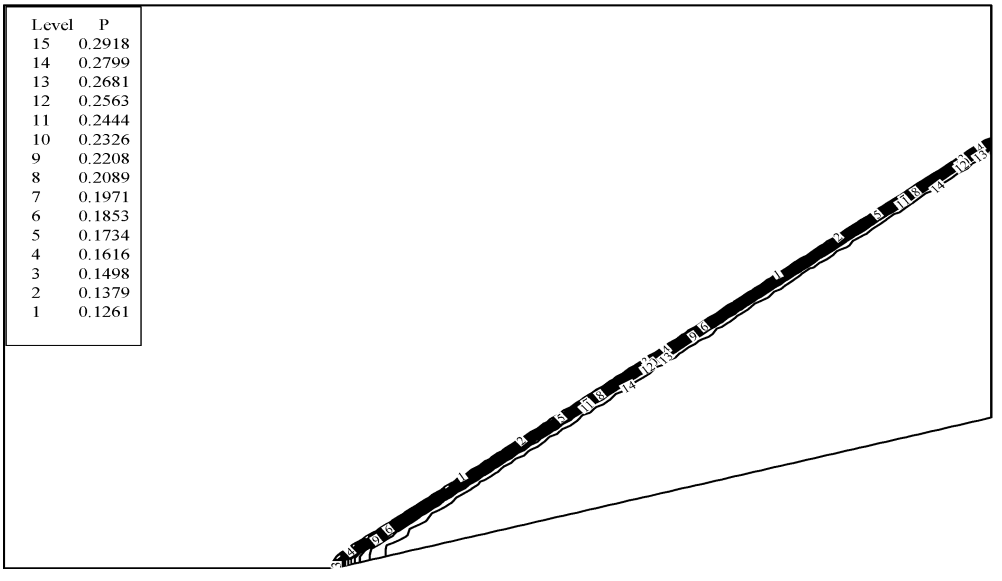

c) S–W scheme

Fig. 2 Pressure contours of supersonic flow past a 15-deg wedge with the creation of an oblique shock.

By the use of the extrapolation relations in Eq. (23), a second-order spatial accurate scheme is produced.

D. Implicit Time Integration Method

For the time integration of all steady-state problems, Euler backward time discretization is adopted. This method is preferable to the multistage Runge–Kutta method because the method evaluates the residual only once per iteration and allows a larger time step to be used.[2] Thus, an implicit method known as the approximate factorization–alternating direction implicit (AF–ADI) scheme is employed for all computations in this paper. When applying the Euler backward time discretization, the governing equations in the computational domain are

$$\left\{ I + \Delta t \left[\frac{\partial}{\partial \xi}(\hat{A}^+ + \hat{A}^-) + \frac{\partial}{\partial \eta}(\hat{B}^+ + \hat{B}^-) \right] \right\}^n \Delta \hat{W}_{i,j} = -\boldsymbol{R}^n_{i,j}$$

$$R^n_{i,j} = \Delta t \left\{ \frac{\partial \hat{F}}{\partial \xi} + \frac{\partial \hat{G}}{\partial \eta} \right\}^n_{i,j} \tag{25}$$

where I is an identity matrix, $\boldsymbol{R}$ is a residual vector, and $\Delta \hat{W}_{i,j} = \hat{W}^{n+1}_{i,j} - \hat{W}^n_{i,j}$. The flux Jacobians denoted by $\hat{A} = \partial \hat{F} / \partial \hat{W}$ and $\hat{B} = \partial \hat{G} / \partial \hat{W}$ in Eq. (25) can be taken as the Jacobian from van Leer's flux. These are given in Ref. 16. The left-hand side of Eq. (25) can be efficiently inverted using the AF–ADI method.[17]

III. Results and Discussion

To investigate the computational characteristics of the gas-kinetic BGK scheme in simulating two-dimensional compressible inviscid flows, three typical flow problems that are found in the literature are tested, namely, a supersonic flow over a wedge, a channel with a 15-deg ramp, and a flow past an impulsively started cylinder. The computed results for the BGK scheme will be compared with the available exact solutions and the numerical results obtained by the use of the Steger–Warming scheme and Roe's scheme. Then, all of the significant features revealed by the schemes will be discussed.

Case 1: Supersonic Flow over a Wedge

This problem deals with a supersonic flow over a wedge with a half angle of 15 deg, and it is taken from Ref. 18. The supersonic flow develops an oblique shock at the leading edge of the wedge. It offers a good opportunity to verify the numerical results against the exact solution, which is computed using the perfect gas equations.

The freestream Mach number M_∞ for this problem is at 2.5, with density ρ_∞ and velocity component U_∞ at 1.0, respectively. The angle of attack for the flow is at 0 deg. The CFL number used for the AF–ADI method is 1.0. A structured grid with 151×101 grid points is used for the current calculation, and it is shown in Fig. 1. There are five sets of boundary conditions for this problem. At inlet, a supersonic flow is realized, where four flow variables ρ, U, V, and p are set to their respective freestream values. Similarly, for the far-field boundary, the four flow variables are also set to freestream values. At supersonic outlet, ρ, U, V, and p are extrapolated from interior points. Last, the lower part of the domain comprises the wall surface of the wedge and the symmetry plane. Thus, at the lower part of the domain, the point starting from the inlet to the leading edge of the wedge is described by a symmetry plane boundary condition, while the rest of it is an inviscid wall boundary condition.

The flow is computed by using a second-order BGK scheme with the AF–ADI method for time integration, and the CFL number adopted is 1.0. The numerical solutions are validated with the exact solution from the literatures and compared with Roe FDS and Steger–Warming FVS schemes. The outcome of this simulation shows that the BGK scheme is able to produce quality solutions. Figure 2 shows the pressure contour plot for the BGK, Roe, and Steger–Warming schemes. Good agreement among the schemes can be seen, except that the contour lines for the Roe and the Steger–Warming schemes diverge slightly around the leading edge of the wedge in comparison with the BGK scheme. In addition to the pressure contour, Fig. 2 shows the Mach and pressure distributions along the lower boundary of the problem for the BGK scheme compared with the exact solution, the Roe scheme, and the Steger–Warming. The Mach number is in Fig. 3, whereas the pressure distribution is in Fig. 4. The comparison made in Fig. 3 shows that the result produced by the Roe scheme is not as accurate as that by the BGK scheme. This is substantiated by the fact that the Roe scheme differs from the exact solution after the shock, whereas the BGK and Steger–Warming (S–W) schemes are able to give accurate solution of the flow. It is also observed that the resolution of the contact discontinuity by the S–W scheme lacks the accuracy of the BGK scheme. Similar remarks can be made regarding the pressure distribution, with the exception that the BGK scheme suffers a small jump after the shock. In Fig. 5, comparison of convergence history

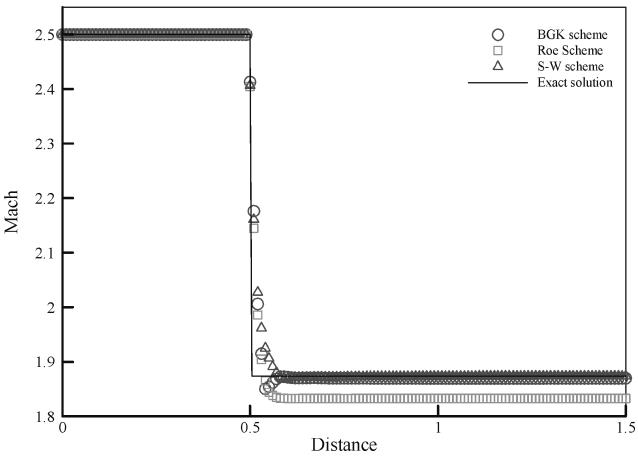

Fig. 3 Mach number along the lower boundary of flow past a 15-deg wedge.

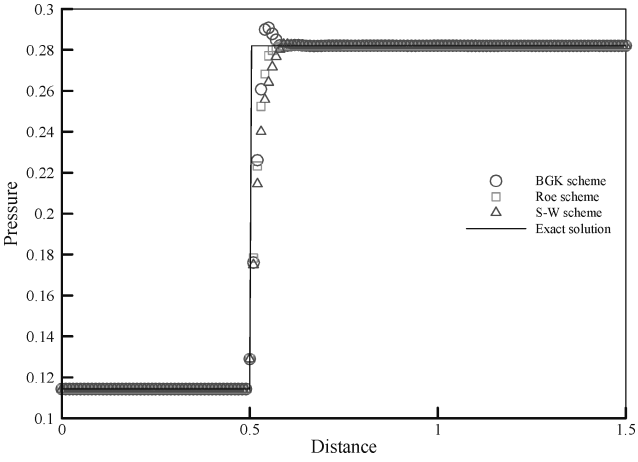

Fig. 4 Pressure along lower boundary of flow past a 15-deg wedge.

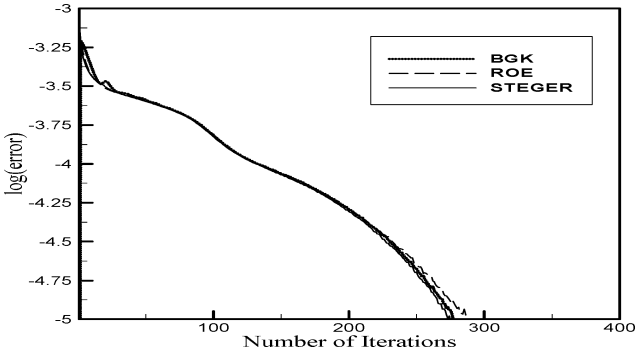

Fig. 5 Convergence history comparison for BGK, Roe, and S–W schemes (wedge).

for the BGK, Roe, and S–W schemes is given. From Fig. 5, it is seen that the BGK scheme has better convergence than Roe's scheme and is comparable to the S–W scheme.

Case 2: Channel with a 15-Degree Ramp

In this case, the steady-state flow is computed for a two-dimensional channel with a 15-deg ramp. There is an attached shock at the compression ramp corner, which reflects from the top wall, forming a Mach stem. The Mach number is chosen so that the extent of the Mach stem is about 20% of the channel height. The shock wave continues to reflect from the bottom and top walls, before exiting the channel. The ramp-shoulder expansion fan acts to weaken the first reflected shock.

The freestream conditions used in this case comprises a 1.8 Mach number at zero angle of attack, with the density and speed of sound set to one unit, respectively. The CFL number is 1. Again, a structured grid for the flow domain is generated with 151×51 points and is shown in Fig. 6. Because the flow at the inlet is supersonic, ρ, U, V, and p are set equal to their respective freestream values. An extrapolation method is applied on ρ, U, V, and p for a supersonic outlet. The top and lower parts of the channel are solid surfaces, where an inviscid wall boundary condition is adopted.

This problem is solved using a second-order BGK scheme with AF–ADI method for time integration along with a CFL number of 1.0. The pressure contours with 15 equally spaced levels are shown in Fig. 7 for the BGK, Roe, and S–W schemes. They show a good agreement with the contour results of Kao and Liou.[19] Figure 8 shows the comparison made between the schemes for the normalized pressure along the lower wall of the channel. The results for all of the schemes are shown to agree very well with each other and with

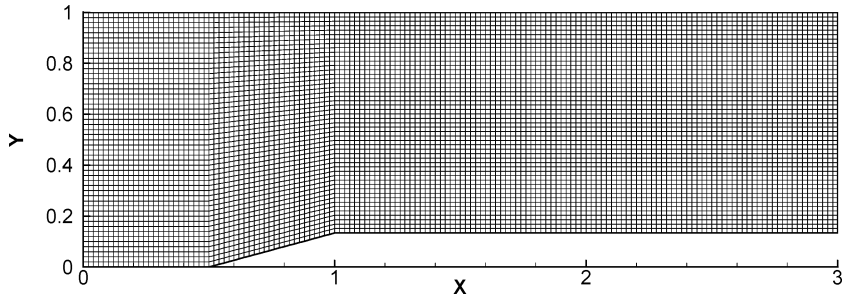

Fig. 6 Grid for two-dimensional channel problem with 151 × 51 grid points.

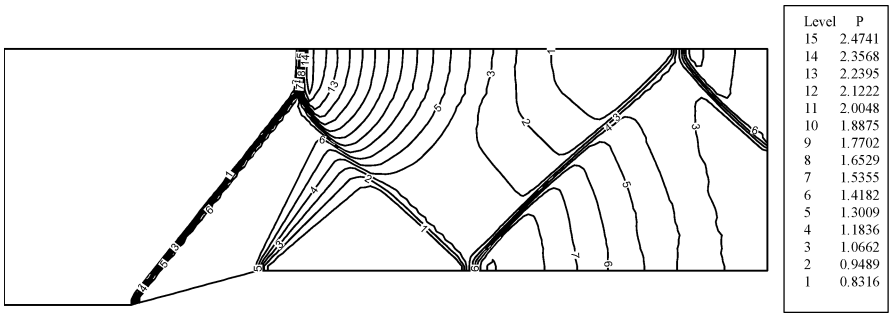

a) BGK scheme

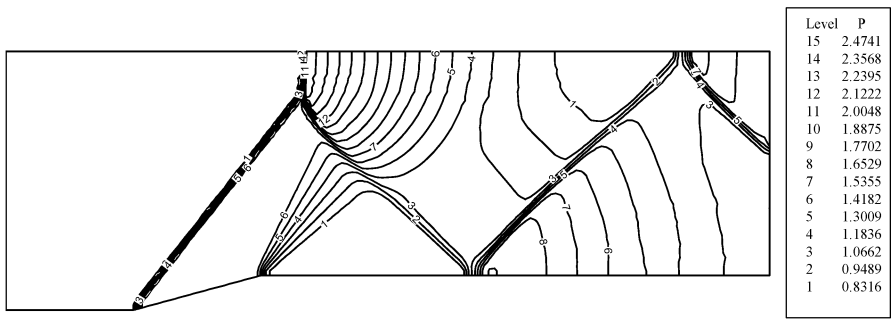

b) Roe scheme

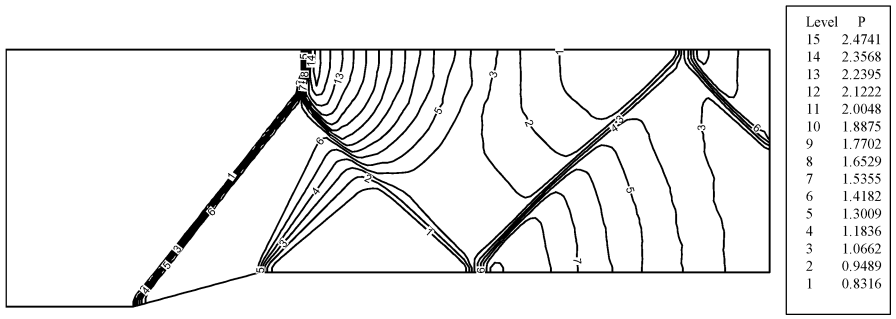

c) S–W scheme

Fig. 7 Pressure contours for channel with 15-deg ramp.

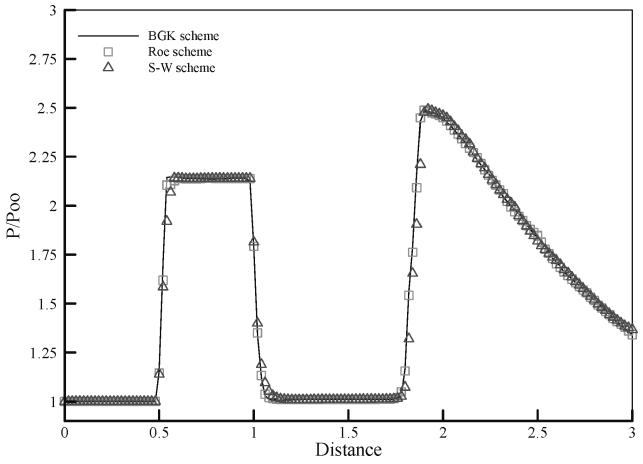

Fig. 8 Normalized pressure along the lower solid wall of the channel.

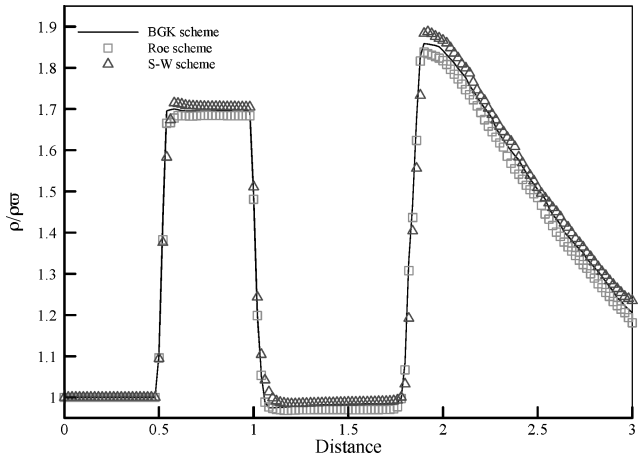

Fig. 9 Normalized density along the lower solid wall of the channel.

the results from Kao and Liou. However, at the first shock location around 0.5, Fig. 8 shows that the BGK scheme exhibits better shock resolution than the other two schemes. The density distributions of the S–W and Roe schemes are also used to verify the BGK scheme in Fig. 9. This comparison clearly shows the superiority of the BGK scheme over both schemes: Shocks are better captured, and the values of the density after the first, second, and third shocks, which are around 1.7, 0.9, and 1.85, respectively, agree very well with the density profile from Kao and Liou[19] in comparison with the other schemes.

Case 3: Impulsively Started Cylinder

This problem involves a steady flow past a cylinder that is started impulsively. This problem is known to be difficult to compute because a region of very low pressure and low density develops at the rear of the cylinder. In such regions, the possibilities of negative pressure and density appearing are very high during the calculations, which break down most numerical schemes. This phenomenon is encountered when the Roe FDS scheme is tried on this problem. Only the BGK scheme and the S–W FVS scheme are able to simulate the flow past the cylinder. Thus, only the numerical results from these two schemes are available for discussions.

The freestream conditions used in this problem comprises a uniform flow at $M = 3.5$ at zero angle of attack, with the density and speed of sound set to one unit. The CFL number being used is one unit. Structured grid for the flow domain is generated by 181×51 points and is given in Fig. 10. At the body surface of the cylinder, an inviscid wall boundary condition is enforced. The boundary condition at the far field is set in such a way that, for a supersonic inflow condition, the flow variables are set to their

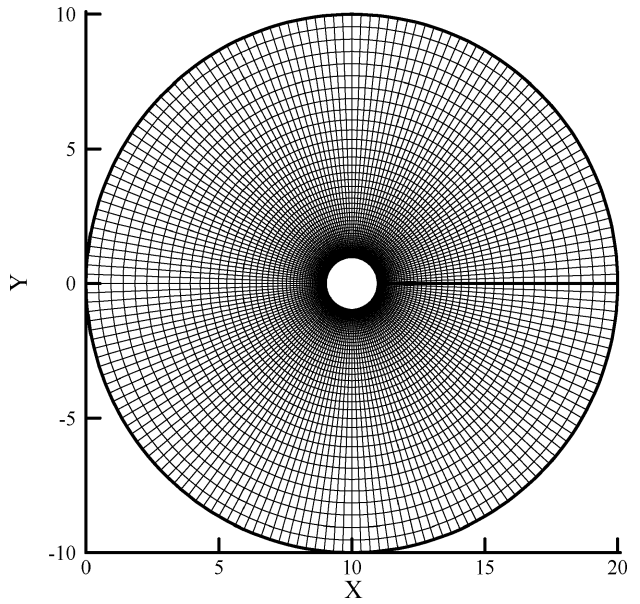

Fig. 10 Grid for cylinder with 181 × 51 points.

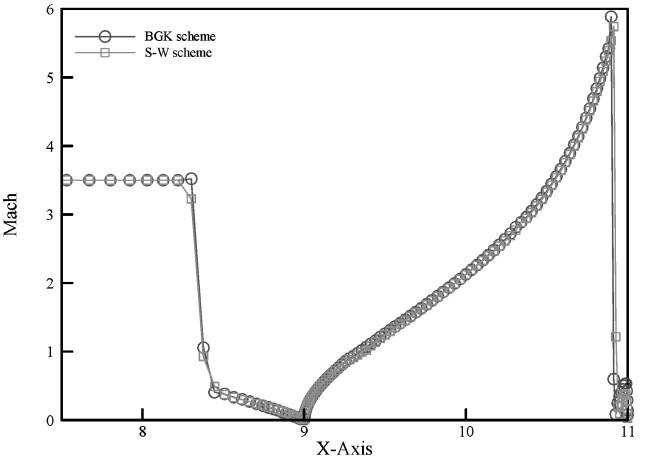

Fig. 11 Mach number on the symmetry line and over the cylinder.

respective freestream conditions, whereas for the supersonic outflow condition, the flow variables are extrapolated from the interior points. At the wake cut boundary of the cylinder O mesh topology, a periodic boundary condition is used.

A converged solution is achieved when the solution is iterated until time $T = 7$ with CFL equal to 1.0 using the AF–ADI method in time integration. Figure 11 shows the computed Mach number distribution along the symmetry line and over the upper surface of the cylinder for the second-order BGK and S–W schemes. The density, pressure, and Mach number contours are also presented in Fig. 12 for the BGK and S–W schemes. Examination of these contour plots revealed that both the sharp bow shock in the front and a V-shaped weak shock behind the cylinder are fairly well captured. Also, the Mach number distribution shows that the expansion in the rear part of the cylinder creates an even higher Mach number, wherein the BGK scheme has a higher Mach number than the S–W scheme results and the results from Choi and Liu.[20] This again indicates that the BGK scheme may yield a less diffusive solution with consequent higher accuracy.

IV. AF–ADI Method vs Runge–Kutta Method

To compare the accuracy of AF–ADI scheme with Runge–Kutta scheme, the impulsively started cylinder problem was selected as a test case. The solution of this problem was obtained using the BGK scheme with both the AF–ADI and Runge–Kutta methods.

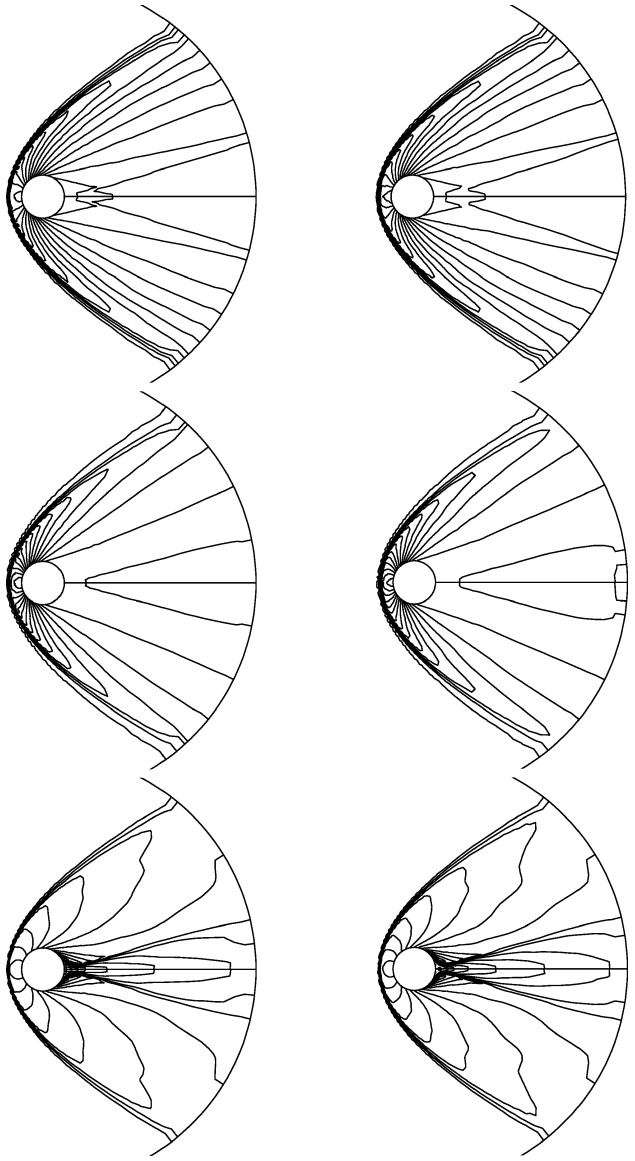

a) Second-order BGK scheme b) Second-order S–W scheme

Fig. 12 Density, pressure, and Mach number contours for flow past a cylinder.

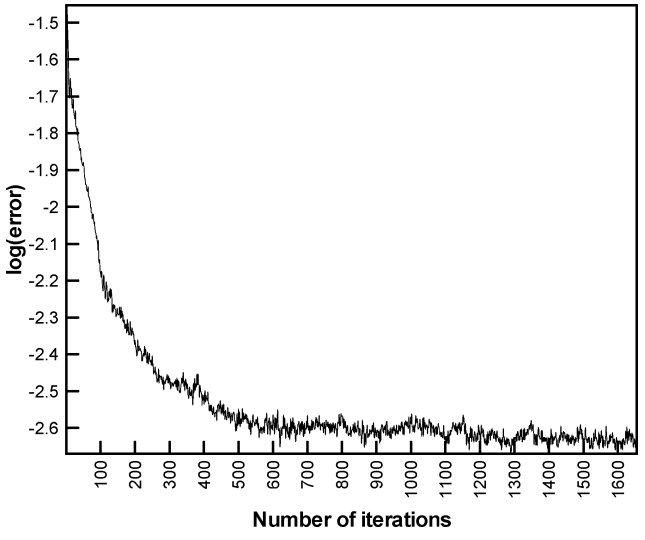

Fig. 13 Convergence history of BGK scheme via Runge–Kutta explicit method for the impulsively started cylinder problem at CFL = 1.2.

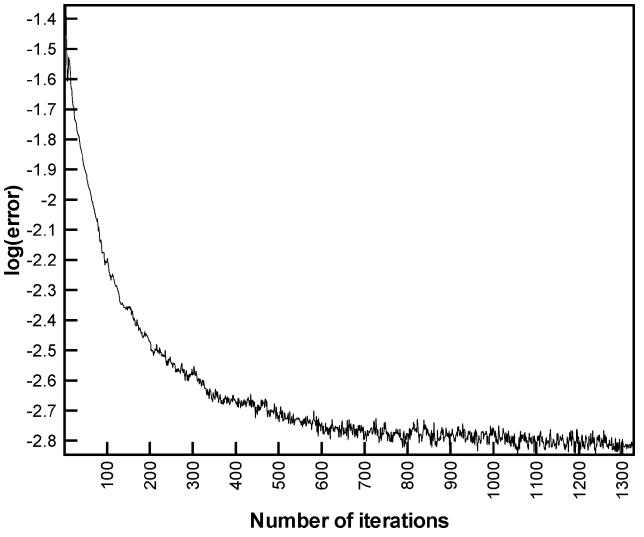

Fig. 14 Convergence history of BGK scheme via AF–ADI implicit method for the impulsively started cylinder problem at CFL = 1.5.

The maximum allowable CFL number for the Runge–Kutta method is 1.2, for which the steady-state solution is reached at time $T = 7$ after 1654 iterations, as shown in Fig. 13. Conversely, the AF–ADI method allows running the algorithm at CFL number greater than 1.5, which yields steady-state solution after 1327 iterations, which is shown in Fig. 14. Thus, Figs. 13 and 14 and the numerics show that when the CFL number is increased the number of iterations that are needed to obtain steady-state solution decreased accordingly. In addition, the implicit method offer great advantage on the stability as compared with the explicit method, as validated by numerical results and the literature.[14,15,21] Although the Runge–Kutta method is simpler to code when compared with the AF–ADI method, it requires more steps for the evaluation of the residuals per iteration, resulting in additional computing time in comparison with the AF–ADI, which evaluates residuals only once per iteration.[2] In a nutshell, the AF–ADI implicit method is preferable to the Runge–Kutta explicit method. In addition, Figs. 13 and 14 shows that the results of AF–ADI implicit method are more accurate than Runge–Kutta method results.

V. Conclusions

The gas-kinetic BGK scheme for the two-dimensional compressible inviscid flow is developed from the Bolzmann equation. The developed BGK scheme is successfully applied to simulate compressible inviscid flow problems. In all of the test cases conducted, the solutions produced by the BGK scheme is less diffusive than the other two schemes tested in this paper. The developed scheme is able to produce numerical results that yield far better shock resolutions. The accuracy of the BGK scheme in simulating the flows has been validated by the numerical results of each problem in this paper. The BGK scheme is also able to simulate flow that contain strong shocks and expansions, as well as subsonic flow region as present in the cylinder problem without breaking down, unlike the popular Roe FDS scheme. Thus, it is concluded that the BGK scheme is able to produce numerical results with better accuracy and high-resolution capabilities to capture shock, rarefaction, and contact discontinuities, and the BGK scheme is robust as compared to other schemes tested in this paper.

The current paper deals with the implementation of the gas-kinetic BGK scheme to compressible inviscid flows. It is the authors' intent to extend the developed BGK scheme to simulate compressible viscous flows in the near future. It is hoped that the results for the viscous flows will be published in coming publications.

Acknowledgment

The authors acknowledge the support of the Ministry of Science, Technology and Environment, Malaysia, under Grant 02-03-02-0017S.

References

[1]Roe, P. L., "Approximate Riemann Solvers, Parameter Vectors and Difference Schemes," *Journal of Computational Physics*, Vol. 43, 1981, pp. 357–372.

[2]Chae, D. S., Kim, C. A., and Rho, O. H., "Development of an Improved Gas-Kinetic BGK Scheme for Inviscid and Viscous Flows," *Journal of Computational Physics*, Vol. 158, 2000, pp. 1–27.

[3]Xu, K., *Gas-Kinetic Scheme for Unsteady Compressible Flow Simulations*, von Kármán Inst. for Fluid Dynamics Lecture Series, Vol. 1998-03, Von Kármán Inst., Rhode St. Genese, Belgium, 1998.

[4]Xu, K., and Lui, S., "Entropy Analysis of Kinetic Flux Vector Splitting Schemes for the Compressible Euler Equations," ICASE Rept. 99-5, Jan. 1999.

[5]Tang, T., and Xu, K., "Gas-Kinetic Schemes for the Compressible Euler Equations I: Positivity-Preserving Analysis," *Zeitschrift für Angewandte Mathematik und Physik*, Vol. 50, 1999, pp. 258–281.

[6]Ong, J. C., Omar, A. A., and Asrar, W., "The Accuracy of Gas-Kinetic Schemes for Solving Compressible Inviscid Flow Problems," Inst. of High Performance Computing, International Conf. on Scientific and Engineering Computation, Singapore, Dec. 2002.

[7]Xu, K., "Gas-Kinetic Theory Based Flux Splitting Method for Ideal Magnetohydrodynamics," ICASE Rept. 98-53, Nov. 1998.

[8]Xu, K., "A Gas-Kinetic BGK Scheme for the Compressible Navier–Stokes Equations and Its Connection with Artificial Dissipation and Godunov Method," *Journal of Computational Physics*, Vol. 171, 2001, pp. 289–335.

[9]Ong, J. C., Omar, A. A., and Asrar, W., "Evaluation of Gas-Kinetic Schemes for Solving 1-D Inviscid Compressible Flow Problems," *International Journal of Computational Engineering Science*, Vol. 4, Dec. 2003, pp. 829–851.

[10]Xu, K., "A Gas-Kinetic Method for Hyperbolic-Elliptic Equations and Its Application in Two-Phase Fluid Flow," ICASE Rept. 99-31, Aug. 1999.

[11]Lian, Y., and Xu, K., "A Gas-Kinetic Scheme for Multi-Material Flows and Its Application in Chemical Reaction," ICASE Rept. 99-28, July 1999.

[12]Ruan, Y., and Jameson, A., "Gas-Kinetic BGK Method for Three-Dimensional Compressible Flows," AIAA Paper 2002-0550, Jan. 2002.

[13]Kunik, M., Qamar, S., and Warnecke, G., "A BGK-Type Flux Vector Splitting Scheme for the Ultra-Relativistic Euler Equations," *Journal of Computational Physics*, Vol. 187, 2003, pp. 572–596.

[14]Hoffmann, K. A., and Chiang, S. T., *Computational Fluid Dynamics for Engineers*, Vol. 1, Engineering Education System, Wichita, KS, 1993, Chaps. 3 and 9.

[15]Hirsch, C., *The Numerical Computation of Internal and External Flows*, Vol. 2, Wiley, New York, 1990, Chap. 21.

[16]Pulliam, T. H., "Notes on Solution Methods in Computational Fluid Dynamics," NASA Ames Research Center, Moffett Field, CA, Jan. 1986.

[17]Hoffmann, K. A., and Chiang, S. T., *Computational Fluid Dynamics for Engineers*, Vol. 2, Engineering Education System, Wichita, KS, 1993, Chap. 12.

[18]John, J. E. A., *Gas Dynamics*, 2nd ed., Prentice–Hall, Upper Saddle River, NJ, 1984, Chap. 9.

[19]Kao, K. H., and Liou, M. S., "Grid Adaptation Using Chimera Composite Overlapping Meshes," *AIAA Journal*, Vol. 32, 1994, pp. 942–949.

[20]Choi, H., and Liu, J. G., "The Reconstruction of Upwind Fluxes for Conservation Laws: Its Behavior in Dynamic and Steady State Calculations," *Journal of Computational Physics*, Vol. 144, 1998, pp. 237–256.

[21]Chung, T. J., *Computational Fluid Dynamics*, Cambridge Univ. Press, Cambridge, England, U.K., 2002, Chap. 4.

C. Kaplan
Associate Editor